



Large-scale preparation of solution-processable one-dimensional V₂O₅ nanobelts with ultrahigh aspect ratio for bifunctional multicolor electrochromic and supercapacitor applications

Sihang Zhang^a, Sheng Chen^{b,*}, Yonghui Luo^b, Bin Yan^b, Yingchun Gu^b, Feng Yang^a, Ya Cao^a

^a State Key Laboratory of Polymer Materials Engineering, Polymer Research Institute of Sichuan University, Chengdu, 610065, China

^b Functional Polymer Materials Laboratory, College of Biomass Science and Engineering, Sichuan University, Chengdu, 610065, China

ARTICLE INFO

Article history:

Received 7 April 2020

Received in revised form

28 May 2020

Accepted 1 June 2020

Available online 5 June 2020

Keywords:

Vanadium pentoxide

Nanobelts

Electrochromism

Supercapacitor

Patterned displays

ABSTRACT

Solution-processable V₂O₅ nanobelts are successfully synthesized by a very simple and large-scale solution treatment method using commercial bulk V₂O₅ powders as precursor. The prepared V₂O₅ nanobelts with lengths up to 20 μm, widths of 10–30 nm, and aspect ratio of over 1000 displays excellent electrochromic and electrochemical capacitance performance. A large optical modulation, rapid switching speed and remarkable cycling stability (sustaining 94% of its initial optical contrast after 1000 cycles) are achieved for V₂O₅ nanobelt film (V₂O₅-nb film). And the V₂O₅-nb film also shows large specific capacitance and excellent capacitance retention (capacitance decay of only 5% after 500 cycles). In addition, the level of stored energy for V₂O₅-nb film could be simultaneously monitored by a reversible and fast color change even at high current charge/discharge conditions (16 A/g). The spray-processable large-scale patterned electrochromic displays based on V₂O₅ nanobelts exhibited various color variation and large optical contrast. The solution-processable V₂O₅ nanobelt shows promising features for applications in energy efficient displays, lithium-ion batteries, supercapacitors and electrochromic devices.

© 2020 Elsevier B.V. All rights reserved.

1. Introduction

Transition metal oxides (TMOs) as versatile materials have attracted extensive attention due to its wide applications in lithium ion battery, sensors, transistors, photocatalysis, supercapacitor and electrochromism [1,2]. One of the most widely studied examples is the vanadium pentoxide (V₂O₅) [3,4]. As a typical transition metal oxide material, V₂O₅ possesses natural abundance, low cost, high density of guest cations and excellent interaction with ions or molecules [5]. And what is more, V₂O₅ owns unique optical and electrochemical properties [6]. These advantages enables V₂O₅ to be applied as promising electrochromic and supercapacitor electrode materials [7]. However, the bulk V₂O₅ with dense morphology suffers from poor electrochemical stability, slow electrochemical kinetics, low electrical conductivity and significant volume expansion during cycling [8,9].

In order to overcome these difficulties, some various methods

have been developed [10,11]. An effective approach is to synthesize nanosized materials [12,13]. Formation of a unique nanostructure is a common and reliable approach for the improvement of electrochromic and capacitance performance [14]. The nanostructured morphology could provide large surface area, abundant active sites and shorten ion diffusion distance [15,16]. Owing to the large surface area of nanostructured materials, the electrolyte can be fully contacted with electroactive materials, which can make ions diffusion easier and provide more active reaction area for charge-transfer reactions [17]. Previous reports indicate that the electrochemical performance of bulk V₂O₅ could be significantly improved by developing various dimensional V₂O₅ nanostructures such as nanowires, nanorods, nanotubes and nanobelts [18]. Tong et al. [19] synthesized three-dimensional coralline V₂O₅ nanorods on an indium-doped tin oxide substrate by combining electrodeposition and annealing treatment method. The coralline V₂O₅ nanorod film exhibits desirable electrochromic cycling stability and short switching time. Bonso et al. [20] prepared the one-dimensional V₂O₅ nanotubes by a sol-gel method. And the V₂O₅ nanotube/exfoliated graphite nanoplatelet composite electrode exhibits

* Corresponding author.

E-mail address: chensheng@scu.edu.cn (S. Chen).

improved electrochemical performance in comparison with its component materials. Wang et al. [21] synthesized V_2O_5 nanowires with ultrahigh aspect ratio by a hydrothermal route using $[VO(O)_2(OH_2)]^+$ as the precursor. The V_2O_5 nanowires show a high specific surface area of $25.6\text{ m}^2/\text{g}$ and specific capacitance of 351 F/g . Yu et al. [22] synthesized mesoporous V_2O_5 nanofibers by combining sol gel processing and electrospinning method. The V_2O_5 nanofibers exhibit improved Li^+ storage capacity of 370 mAh/g and high charge/discharge rate of up to 800 mA/g . However, these preparation methods of V_2O_5 nanostructures are not suitable for large scale production because of high cost, rigorous operation condition and low yield. The development of large-scale production with low cost, ease of synthesis and green chemistry for nanostructured V_2O_5 materials is still a great challenge [23].

Herein, a simple, low cost and high yield method was demonstrated for the large-scale preparation of V_2O_5 nanobelts with ultrahigh aspect ratio. The solution-processable V_2O_5 nanobelts were successfully synthesized by vigorous stirring the commercial V_2O_5 powder in NaNO_3 solution under room temperature. The preparation procedures do not require expensive precursors and rigorous operation conditions. This method is very promising for realizing industrial production of V_2O_5 nanobelts. Owing to the unique nanostructured morphology, the V_2O_5 nanobelts with ultrahigh aspect ratio were suitable for electrochromic and supercapacitor applications. And the V_2O_5 nanobelts exhibits significantly improved electrochromic and electrochemical capacitance performance compared with commercial bulk V_2O_5 powder. In addition, it is demonstrated that the level of stored energy for V_2O_5 -nb film could be simultaneously monitored by a reversible and fast color change even at high current charge/discharge conditions (16 A/g). Finally, the spray-processable V_2O_5 nanobelt-based patterned electrochromic display with an area of 36 cm^2 was successfully fabricated and exhibited various color variation, fast response speed and large optical contrast.

2. Experimental

2.1. Materials

Bulk V_2O_5 powder and poly (3,4-ethylenedioxythiophene)-poly (styrenesulfonate) (PEDOT:PSS, 1.0 wt%) aqueous dispersion were bought from Sigma-Aldrich. NaNO_3 powder was purchased from Chengdu Kelong Chemical Reagent Factory. LiClO_4 , Poly (methyl methacrylate) (PMMA) and Propylene carbonate (PC) were provided by Chengdu Hua-xia Chemicals Co., Ltd. Indium tin oxide (ITO) conductive glass was obtained from Shenzhen South China XiangCheng Science & Technology Co., Ltd.

2.2. Synthesis of V_2O_5 nanobelts

The V_2O_5 nanobelts were synthesized by a simple solution treatment process. The detailed procedures were described as follow. 5 g commercial V_2O_5 powder and 500 ml 1.5 M NaNO_3 solution were add into the three-neck flask. The mixture was vigorously stirred at ambient temperature for 7 days. During the reaction, the solution gradually changed from yellow to reddish brown. Then the products were washed by centrifugation-redispersion cycles with ultrapure water. After that, the solid content of the V_2O_5 nanobelt aqueous dispersion was 2.0%. And the yield of obtained V_2O_5 nanobelts can be calculated to over 80% according to formulas.

2.3. Fabrication of V_2O_5 nanobelt electrode and device assembly

The V_2O_5 nanobelt film electrode was fabricated by spray-

coating V_2O_5 nanobelt aqueous dispersion onto the heated ITO conductive glass. And the V_2O_5 film electrode was constructed in air atmosphere without the protection of inert gas. In order to remove the moisture, the V_2O_5 film electrode is dried on the hot-table at 70°C for 1 h after spraying. For comparison, the pristine bulk V_2O_5 film electrode was fabricated by the same method. The LiClO_4 -PMMA-PC gel electrolyte (GE) was synthesized according to our previous report [24]. For patterned device assembly, 600 μL gel electrolyte was uniformly deposited on the surface of spray-coated V_2O_5 -nb film and spray-coated PEDOT:PSS film electrode. The two electrodes were carefully pressed against each other to obtain good adhesion. Then the four sides of the device were sealed by epoxy glue. The device was assembled under ambient condition. The masks were covered onto the ITO conductive glass to form various patterns in the spraying process. The large-scale patterned electrochromic device ($6.0\text{ cm} \times 6.0\text{ cm}$) presented the following configuration:

Glass/ITO/ V_2O_5 -nb/GE/PEDOT:PSS/ITO/Glass.

The electrochromic properties of large-size patterned device were characterized in the sample compartment of a spectrophotometer and connected a two-electrode system to an electrochemical workstation.

2.4. Characterization

The morphologies of commercial V_2O_5 and V_2O_5 -nb films were performed by SEM (JSM-5900LV, FEI) and TEM (G^2 -F20, FEI). The element mapping of V_2O_5 nanobelts was carried out by energy dispersive X-ray spectroscopy (EDS mapping, JSM-5900LV, FEI). The chemical structures of commercial V_2O_5 and V_2O_5 -nb films were clearly measured by FT-IR spectrometer (Tracer-100, Shimadzu) and X-ray powder diffractometer (XRD, D/max-RB, Shimadzu). X-ray photoelectron spectroscopy (XPS) measurements were carried out with a ESCALAB Xi + system using Al ka radiation (Thermo-scientific Co., Ltd). N_2 adsorption was determined by BET (Brunauer-Emmett-Teller) measurements using a NOVA-1000e surface area analyzer. The electrochemical performance of the films was conducted on a three-electrode system. And the 1.0 M LiClO_4/PC solution was used as the electrolyte. The V_2O_5 nanobelt coated ITO substrates were served as working electrode, the platinum sheet as counter electrode and the saturated calomel electrode as reference electrode. The three-electrode system based on V_2O_5 film electrode was placed in the sample compartment of a spectrophotometer and connected to an electrochemical workstation, both interfaced to computers. The CV and galvanostatic charge-discharge curves of the samples were conducted on an electrochemical workstation (CS150, Wuhan Corrtest Instrument Co., Ltd.). The optical responses of the films were recorded by a UV-vis spectrophotometer (TU-1900, Beijing Purkinje General Instrument Co. Ltd.). Electrochemical impedance spectrum (EIS) was carried out on the electrochemical workstation with superimposed 5 mV sinusoidal potential in the frequency range of 0.01–100,000 Hz.

3. Results and discussion

The V_2O_5 nanobelt with high aspect ratio was successfully synthesized by a simple solution treatment method. The typical preparation process of V_2O_5 nanobelt was schematically illustrated in Fig. 1a. And the morphology of pristine bulk V_2O_5 and V_2O_5 nanobelt was clearly displayed in Fig. 1. It can be seen that the commercial bulk V_2O_5 exhibit stone-like dense morphology, as illustrated in Fig. 1 b, d. The bulk V_2O_5 closely piled together to form a compact structure. And the length of single commercial V_2O_5 up to several micrometers. The diameter of the bulk commercial V_2O_5 ranges from 500 nm to 1 μm . The morphology of V_2O_5 nanobelt was

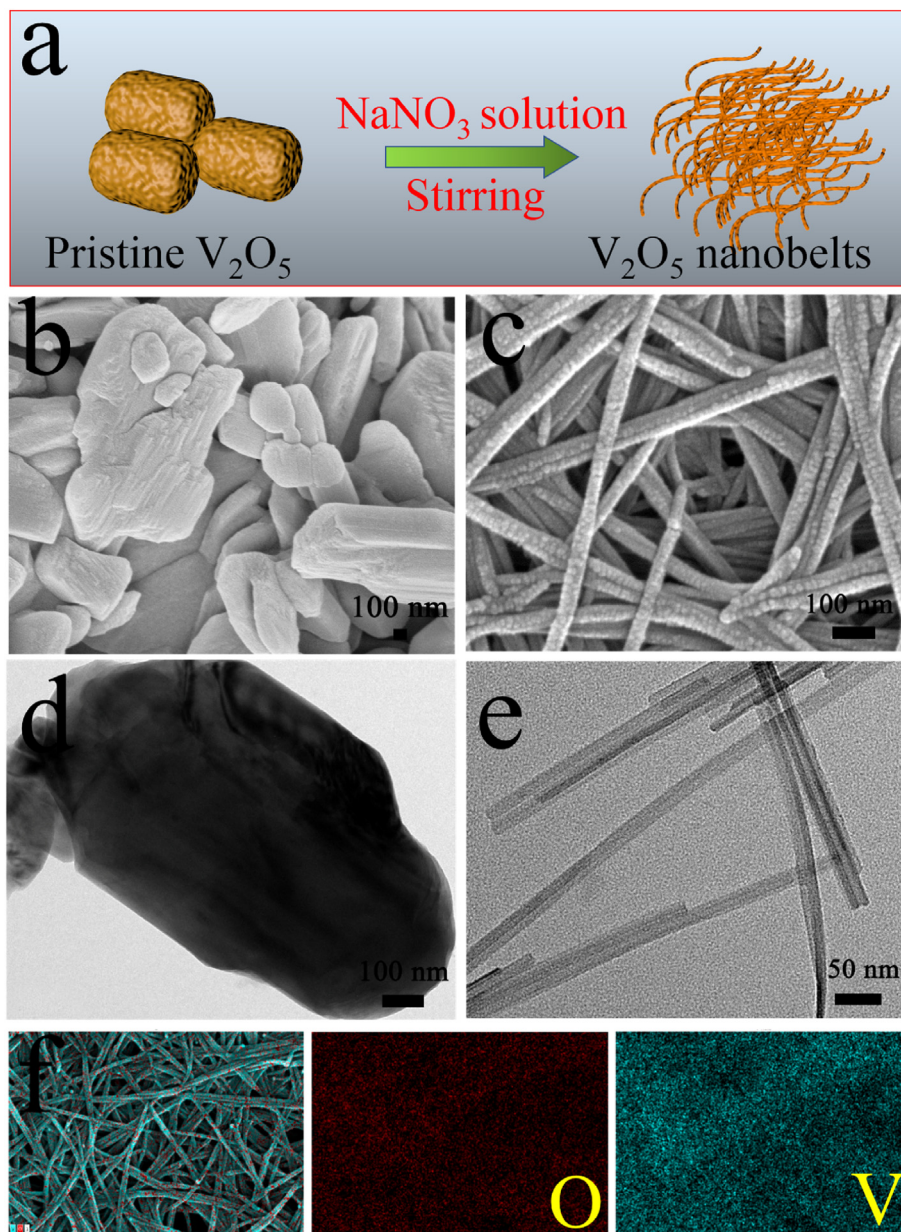


Fig. 1. (a) A schematic illustration of the preparation process of V_2O_5 nanobelts. SEM images of pristine V_2O_5 (b) and V_2O_5 nanobelts (c). TEM images of pristine V_2O_5 (d) and V_2O_5 nanobelts (e). (f) EDS mapping of V_2O_5 nanobelts.

depicted in Fig. 1 c, e, the as-prepared nanosized V_2O_5 exhibits obvious nanobelt morphology and highly uniform in shape. The width of the V_2O_5 nanobelt range from 10 to 30 nm. The length of V_2O_5 nanobelt is over 20 μm , as depicted in the low-magnification TEM image (Fig. S1). From Fig. 1c, the V_2O_5 nanobelts with ultrahigh aspect ratio are easy to form a well-connected networked highly porous structures, which is beneficial for ion diffusion process during the electrochemical reaction. The cross-section SEM images of commercial V_2O_5 and V_2O_5 nanobelts were depicted in Fig. S2, it can be seen that the film thickness of spray-coated pristine V_2O_5 and V_2O_5 nanobelt films are 690 and 800 nm, respectively. The SEM EDS spectrum of the V_2O_5 nanobelts was depicted in Fig. S3. Except for the component elements of spray-coated gold nanoparticles dispersion (to increase the conductivity of sample) and aluminum sheet substrate, the element peaks of V and O were observed in the EDS spectrum of V_2O_5 nanobelt. And the EDS element mapping of

V_2O_5 nanobelts was displayed in Fig. 1f. The result reveals that the presence and uniform distribution of V and O. These results demonstrate that the V_2O_5 nanobelts was successfully synthesized.

The FTIR transmittance spectra of commercial V_2O_5 and V_2O_5 nanobelts were illustrated in Fig. 2a the commercial V_2O_5 and V_2O_5 nanobelts show similar FTIR spectra. The characteristic peak at 1570 and 3500 cm^{-1} were ascribed to the bending and stretching vibrations of water molecules [25]. The absorbance band at 1020 cm^{-1} is attributed to the stretching vibration of $V=O$. The characteristic bands at 590 cm^{-1} and 780 cm^{-1} are associated to the symmetric and asymmetric stretching modes of $V-O-V$ [26]. The XRD patterns of commercial V_2O_5 powder and V_2O_5 nanobelts were presented in Fig. 2b. The characteristic peaks of commercial V_2O_5 powder are located at 15.5, 20.5, 21.8, 26.4, 31.2, 32.5, 33.5, 34.4, 41.5, 42.2, 45.7, 47.5, 51.3, 55.8, 56.4 and 59.0°, corresponding to (200), (001), (101), (110), (301), (011), (111), (310), (002), (102),

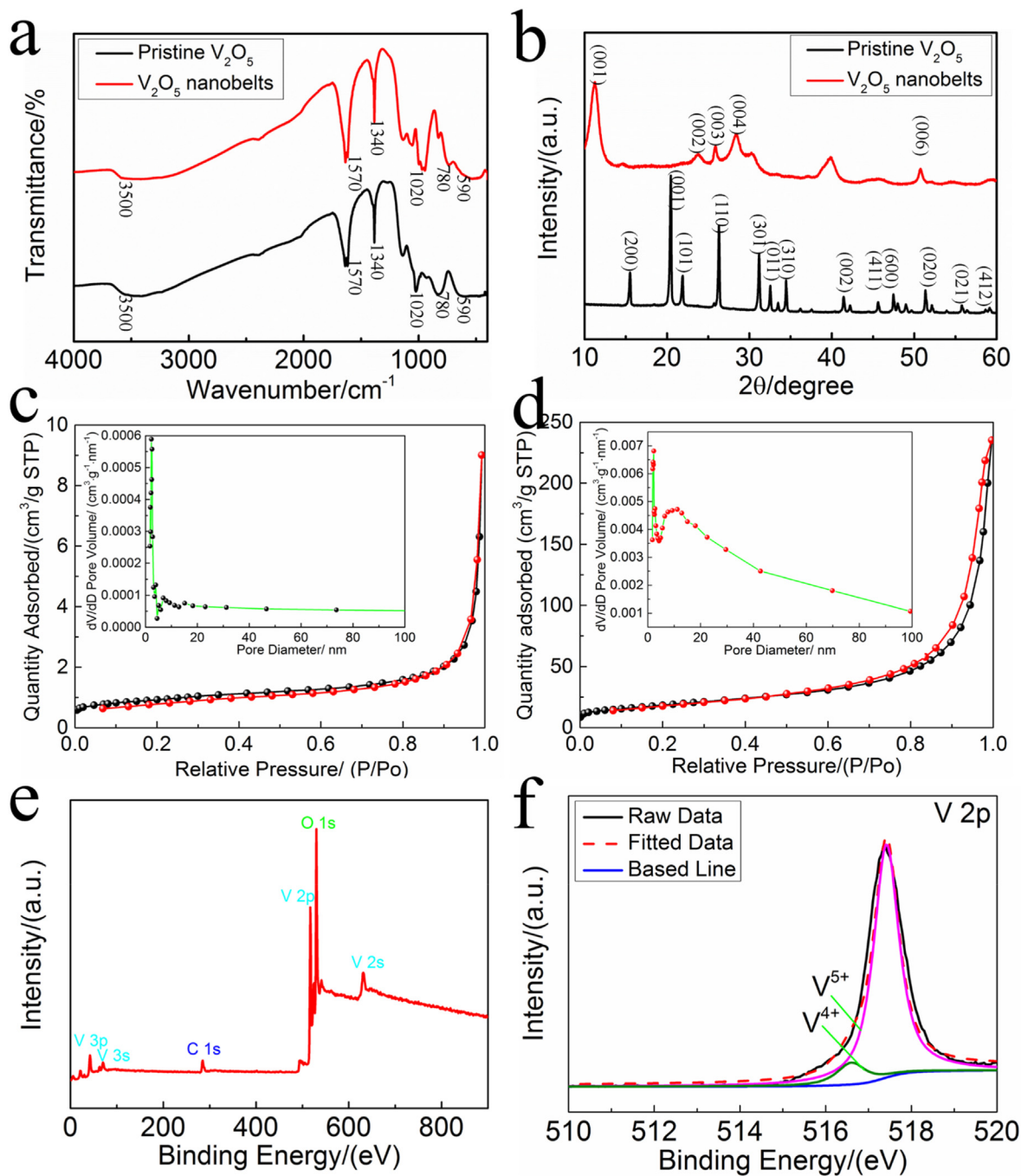


Fig. 2. (a) FTIR spectra of pristine V_2O_5 and V_2O_5 nanobelts (b) XRD patterns of pristine V_2O_5 and V_2O_5 nanobelts. (c, d) Nitrogen adsorption isotherms curves of commercial bulk V_2O_5 (c) and V_2O_5 nanobelts (d) at 77 K. (The insets are the pore size distributions of commercial bulk V_2O_5 and V_2O_5 nanobelts). (e) XPS survey spectra of V_2O_5 nanobelts. (f) XPS V 2p spectra of V_2O_5 nanobelts.

(411), (600), (020), (021), (121) and (412) lattice planes of single phase orthogonal V_2O_5 (space group: Pmmn(59); JCPDS card No. 41–1426), which is consistent with the published literature [27]. The characteristic bands of as-prepared V_2O_5 nanobelts at 11.2, 23.7, 25.8, 28.3 and 50.8°, corresponding to (001), (002), (003), (004) and (006) lattice planes of pure layered hydrated V_2O_5 phase (JCPDS card No. 40–1296). This result is in accordance with the reported literature [26,28]. The difference between the two XRD patterns may be attributed to the presence of structural water in the V_2O_5 nanobelts [25]. The nitrogen adsorption isotherms curves of commercial bulk V_2O_5 and V_2O_5 nanobelts at 77 K as shown in Fig. 2 c,d.

The pore size distributions of commercial bulk V_2O_5 and V_2O_5 nanobelts were shown in the insets of Fig. 2 c,d. The detailed BET parameters of commercial bulk V_2O_5 and V_2O_5 nanobelts were summarized in Table 1. The results show that the surface area of commercial V_2O_5 and V_2O_5 nanobelts is 3.3 and 66.7 m^2/g , respectively (Fig. 2 c,d). And the pore size distribution curves of commercial V_2O_5 and V_2O_5 nanobelts exhibit peaks at 14.3 and 19.6 nm, respectively (the insets of Fig. 2 c,d). The improved surface area of as-prepared V_2O_5 nanobelts is attributed to the interweaved superfine V_2O_5 nanobelts, formation of highly porous nanostructures. The BET measurement results are consistent with the

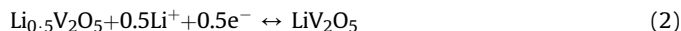
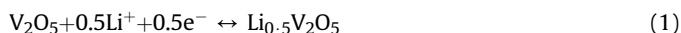
Table 1

The BET parameters of commercial bulk V_2O_5 and V_2O_5 nanobelts (micropore area is obtained according to t-plot; Pore volume is obtained according to BJH adsorption cumulative volume of pores).

Sample	Surface area/(m^2/g)	Micropore area/(m^2/g)	Pore Volume/(cm^3/g)	Micropore volume/(cm^3/g)	Pore size/(nm)
Commercial V_2O_5	3.3	0.84	0.012	0.00036	14.3
V_2O_5 nanobelts	66.7	2.63	0.33	0.00030	19.6

SEM and TEM analysis. The XPS survey spectra of commercial bulk V_2O_5 and V_2O_5 nanobelts were illustrated in Fig. S4a and Fig. 2e. The XPS spectra of the two samples are almost the same. And it is shown that only photoelectrons of C, V and O elements were observed for both samples. The existence of carbon element may be attributed to the carbonaceous molecules in the air, and V and O elements were from the V_2O_5 molecules [19]. The XPS $\text{V}2\text{p}$ spectra of the two samples is composed of two components located at 516.5 and 517.3 eV, as displayed in Fig. S4b and Fig. 2f. This result is consistent with reported literatures [26]. The two binding energy values can be assigned to two formal oxidation degrees, V^{5+} and V^{4+} [29,30]. According to the quantitative analysis of XPS survey spectra, the PP atom% of the O, V and C for V_2O_5 nanobelts are 64.15%, 25.47% and 10.38%, respectively. In other words, the calculated ratio of V and O elements is calculated to be 0.4, matching the stoichiometric value of V_2O_5 . It is fully demonstrated that V_2O_5 nanobelts were successfully synthesized.

The electrochemical properties of commercial V_2O_5 and V_2O_5 nanobelt films were characterized by CV curves, as shown in Fig. 3a. Here, the as-prepared V_2O_5 nanobelt film was referred as V_2O_5 -nb film. The CV curves of the films were measured in 1 M LiClO_4/PC solution at 100 mV/s in the potential range of -0.6 – $+1.0$ V the redox peak of commercial bulk V_2O_5 film is not obvious. It is evident that the commercial V_2O_5 film exhibits poor electrochemical performance. When the applied potential is over 0.6 V, the irreversible redox reaction occurs in the commercial bulk V_2O_5 film. It reveals that the commercial bulk V_2O_5 film is not suitable for electrochromic field. The CV curves of V_2O_5 -nb film show two pairs of redox peaks. The redox couple (B/B') is attributed to the reduction of partial V^{5+} ions to V^{4+} state [31]. The color of the V_2O_5 -nb film changed from brick-red to yellow. The redox couple (A/A') is ascribed to the complete conversion of the rest V^{5+} ions to V^{4+} state [32]. The color of the V_2O_5 -nb film changed from yellow to grey. The corresponding oxidation/reduction conversions of V_2O_5 -nb film are shown as follow.



The photographic images of commercial V_2O_5 and V_2O_5 -nb films under different potentials were displayed in Fig. 3b. The color change of commercial bulk V_2O_5 film is almost invisible in the potential range of -0.6 – $+1.0$ V. In contrast, the V_2O_5 -nb film exhibited multiple colors, changing from brick-red ($+1.0$ V), yellow ($+0.2$ V) to grey (-0.6 V). It is evident that the V_2O_5 -nb film show significantly improved electrochromic performance compared to commercial bulk V_2O_5 film.

The optical transmittance spectra of commercial bulk V_2O_5 and V_2O_5 -nb films in the potential range of -0.6 – $+1.0$ V were depicted in Fig. 4a and b. When the potential switched from -0.6 to $+0.9$ V, the optical modulation of commercial V_2O_5 film was nearly negligible. On the contrary, the V_2O_5 -nb film exhibits large optical modulation in the potential range of -0.6 – $+0.9$ V. It is evident that the transmittance of V_2O_5 -nb film decreases significantly as the applied potential increases from -0.6 to $+0.9$ V in the wavelength range of 350–550 nm. The current and corresponding in situ transmittance response of commercial V_2O_5 and V_2O_5 -nb films at 490 nm when potential switched from -0.6 to $+0.9$ V for 10 s per step were presented in Fig. 4 c,d. From the current response curve, the V_2O_5 -nb film exhibited a larger transient current density than bulk V_2O_5 film, reflecting the existence of more active sites for ion diffusion [33]. And the current density of V_2O_5 -nb film reached to the maximum value in shorter time than bulk V_2O_5 film, indicating faster reaction kinetics [34]. From the optical response curve, the optical contrast ($\Delta T = T_b - T_c$, where T_b and T_c represent the transmittance value at bleached and colored state) of V_2O_5 -nb film is calculated to be 41.6% at 490 nm, significantly larger than that of commercial V_2O_5 film (3.8% at 490 nm). The response time (τ) was calculated as the time required for a system to reach 90% of its full transmittance modulation at a certain wavelength [35]. It can be calculated that the response times for bleaching and coloring process are 4.2 and 1.4 s for V_2O_5 -nb film, remarkably shorter than that of commercial bulk V_2O_5 film (8.5 s for bleaching, 6.6 s for coloring). This result is consistent with the analysis of current

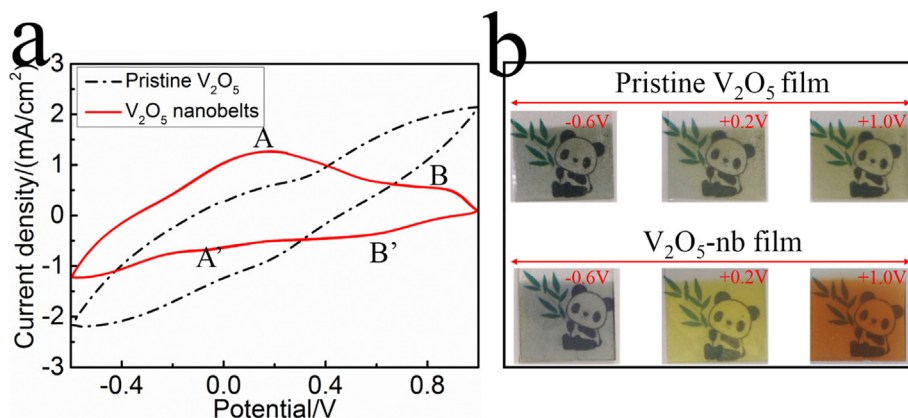


Fig. 3. (a) CV curves of pristine bulk V_2O_5 and V_2O_5 -nb films at 100 mV/s in 1 M LiClO_4/PC electrolyte. (b) Photographs of pristine bulk V_2O_5 and V_2O_5 -nb films at different applied potentials.

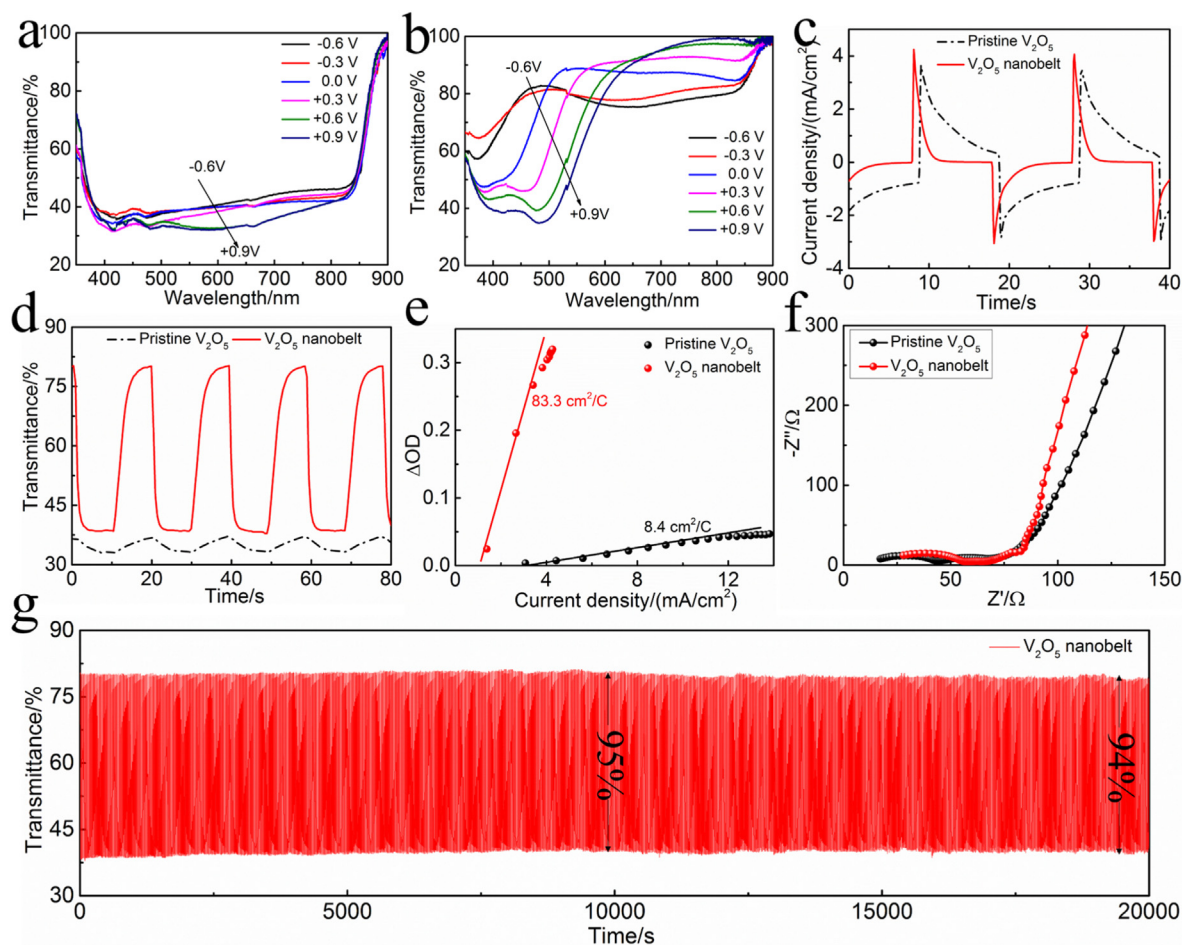


Fig. 4. Transmittance spectra of commercial V_2O_5 (a) and V_2O_5 -nb (b) films under different potentials. Current (c) and optical (d) response of commercial V_2O_5 and V_2O_5 -nb films at 490 nm (-0.6 – $+0.9$ V, 10 s per step). (e) Variation of the optical density (OD) vs. charge density for commercial bulk V_2O_5 and V_2O_5 -nb films. (f) Nyquist plots of commercial bulk V_2O_5 and V_2O_5 -nb films in the frequency range of 0.01–100,000 Hz. (g) Cycling stability of pristine V_2O_5 and V_2O_5 -nb films at 490 nm for 1000 cycles (-0.6 – $+0.9$ V, 10 s per step).

response curve. Coloration efficiency (CE) is a very important parameter for evaluating the electrochromic performance of films. CE is defined as the variation in optical density (ΔOD) per unit charge (Q) inserted/extracted from the electrochromic film [36]. A high CE value denotes that the films provides large optical contrast with small charge insertion/extraction. CE can be calculated from the standard equation as follows [37,38].

$$CE = \Delta OD / Q \quad (3)$$

$$\Delta OD = \log(T_b / T_c) \quad (4)$$

In order to obtain the CE value, the optical density at 490 nm vs. the inserted charge density during the coloration process was presented in Fig. 4e. From the slope of curves, the calculated CE value is $83.3 \text{ cm}^2/\text{C}$ for V_2O_5 -nb film at 490 nm, much higher than that of commercial bulk V_2O_5 film ($8.4 \text{ cm}^2/\text{C}$ at 490 nm). Table 2 summarized the electrochromic parameters of commercial V_2O_5

and V_2O_5 -nb films. EIS is a sensitive and nondestructive measurement, commonly applied in the characterization of electrode [39]. The Nyquist plots of commercial V_2O_5 and V_2O_5 -nb films in 1.0 M LiClO_4/PC solution were illustrated in Fig. 4f. And the equivalent circuit for fitting the electrochemical impedance spectra was displayed in Fig. S5. Both of the films consist of a depressed arc in high frequency region and an inclined line in the low frequency region. It is well accepted that the larger semicircle indicates a higher charge-transfer resistance, and a steeper slope means a fast ion diffusion rate [40,41]. According to the Nyquist plots, the V_2O_5 -nb film shows smaller semicircle and steeper slope than pristine bulk V_2O_5 film. It is evident that the V_2O_5 -nb film exhibits lower charge-transfer resistance and faster ion diffusion rate than commercial bulk V_2O_5 film. The cycling stability of V_2O_5 -nb films at 490 nm with continuously stepping potential at -0.6 and $+0.9$ V (10 s per step) for 1000 cycles was depicted in Fig. 4g. The durability of commercial V_2O_5 film at 490 nm for 50 cycles was displayed in Fig. S6. The optical contrast of commercial V_2O_5 film always sustains at a very

Table 2
Electrochromic performance of pristine V_2O_5 and V_2O_5 -nb films under same operation condition.

Film	Operation condition	λ/nm	T_b/T_c	ΔT (%)	τ_c/s	τ_b/s	CE (cm^2/C)
V_2O_5	-0.6 – $+0.9$ V	490	36.9/33.1	3.8	6.6	8.5	8.4
V_2O_5 -nb	-0.6 – $+0.9$ V	490	80.1/38.5	41.6	1.4	4.2	83.3

low value during cycling, and therefore the commercial V_2O_5 film is not suitable for practical application in electrochromism. The V_2O_5 -nb film sustains 95% of its initial optical contrast after subjected for 500 cycles. And the V_2O_5 -nb film exhibit a high optical contrast of 39.1% and sustain 94% of its original optical contrast even when subjected to 1000 cycles. The result indicates that the V_2O_5 -nb film owns very excellent cycling stability. The improved electrochromic performance of V_2O_5 -nb film is mainly attributed to the special nanobelt structure, which could make ion diffusion easier and provide large surface area for charge-transfer reactions [42,43]. The high optical contrast, fast response speed and excellent cycling stability of V_2O_5 -nb film are very impressive when compared with those of V_2O_5 -related electrochromic films reported in literatures. Table S1 summarizes the electrochromic parameters of previously reported V_2O_5 -related films and the present V_2O_5 -nb film.

The CV curves of commercial V_2O_5 and as-prepared V_2O_5 nanobelt film in a 1.0 M $LiClO_4/PC$ electrolyte solution at different scanning rates ranging from 5 to 200 mV/s were characterized, as shown in Fig. 5. The mass of the spray-coated active materials for both electrodes is about 1 mg. And the electroactive area of the electrode is 1.5 cm \times 2.0 cm. Hence, the mass loading of the pristine V_2O_5 and V_2O_5 -nb film electrode is calculated to be 0.33 mg/cm². A pair of obvious redox current peaks with symmetrical shape was clearly observed in both CV curves. It is well-known that CV curves appear nearly rectangular for electric double-layer capacitors and redox current peaks for pseudocapacitor [41,44]. It is shown that a typical pseudocapacitive behavior arising from the reversible Faradaic redox reactions between V^{5+} and V^{4+} for both of film electrodes. The symmetric redox peaks show that the redox reaction reversibility of both film electrode is very good. As the scanning rate increases from 5 to 200 mV/s, the peak current density increases with a shift of oxidation peak to a more positive position and reduction peaks to a negative position due to the internal resistance of film electrode. And the shapes of well-defined redox reaction peaks are still maintained even when subjecting to a high scanning rate of 200 mV/s. The results demonstrate that the two film electrodes possess low internal resistance, fast charge transfer speed and good electrochemical capacitive nature [32,36]. However, the V_2O_5 -nb film exhibits higher peak current density in comparison with commercial bulk V_2O_5 film, indicating the higher electrochemical activity of V_2O_5 -nb film [45,46].

The electrochemical capacitance performance of commercial V_2O_5 and V_2O_5 -nb films was studied by galvanostatic charge-discharge (GCD) measurement. The specific capacitances of the active films were calculated according to the GCD curves. The

standard formula was presented as follow [47].

$$C = (I \cdot \Delta t) / (m \cdot \Delta V) \quad (5)$$

Where C (F/g) is the capacitance, I (A) is the discharge current, Δt (s) is the discharge time, m (g) is the weight of active materials and ΔV (V) is the potential window (excluding IR drop in the beginning of the discharge). The GCD curves of commercial V_2O_5 and V_2O_5 -nb films under different current densities were depicted in Fig. 6 a,c. The specific capacitance of commercial V_2O_5 and V_2O_5 -nb films as a function of the current density was displayed in Fig. 6 b, d. The non-linear GCD curve of commercial bulk V_2O_5 may be attributed to the dense morphology, leading to very slow charge-transfer reaction and irreversible redox reactions. The specific capacitance of V_2O_5 -nb film is calculated to be 132.5 F/g at a current density of 1.0 A/g, significantly higher than that of commercial V_2O_5 film (45.1 F/g at 1.0 A/g). And the specific capacitance of V_2O_5 -nb film is eleven times larger than commercial bulk V_2O_5 film even at a high current density of 4.0 A/g. It can be seen that the specific capacitance of commercial bulk V_2O_5 film decreased significantly with increasing current density. This is because some active sites of the active materials become inaccessible for charge storage owing to the slow diffusion rate, limiting the migration of the active ions at high current density [44]. And the specific capacitance of V_2O_5 -nb film decreases to 115 F/g as the current density increases to 8.0 A/g. The V_2O_5 -nb film sustains a capacitance of 87.1% at 8.0 A/g, compared to its initial capacitance at 1.0 A/g, indicating an excellent rate capacity and capacitive behaviors at high current density [41]. Long-term electrochemical capacitance retention of commercial V_2O_5 and V_2O_5 -nb films was characterized at a high current density of 16 A/g using GCD measurements for 500 cycles, as illustrated in Fig. S7 and Fig. 6e. The commercial bulk V_2O_5 film retained 88% of its original capacitance value after cycling 100 cycles. In addition, the commercial bulk V_2O_5 film sustains only 73% of its initial capacitance value after subjecting 500 cycles. On the contrary, the V_2O_5 -nb film sustains 97% of its initial capacitance after 100 cycles. Moreover, the capacitance of V_2O_5 -nb film decreased only 5% of initial capacitance even when subjected to 500 cycles. The decreased capacitance value of V_2O_5 -nb film may be attributed to the existence of irreversible reaction during cycling and the active materials peel from the ITO glass substrates due to the shrinking and expanding during cycling redox reactions [48,49]. It is demonstrated that V_2O_5 -nb film possesses very excellent electrochemical capacitance durability. The improved capacitance properties of V_2O_5 -nb film are mainly attributed to the unique nanobelt structures, which can

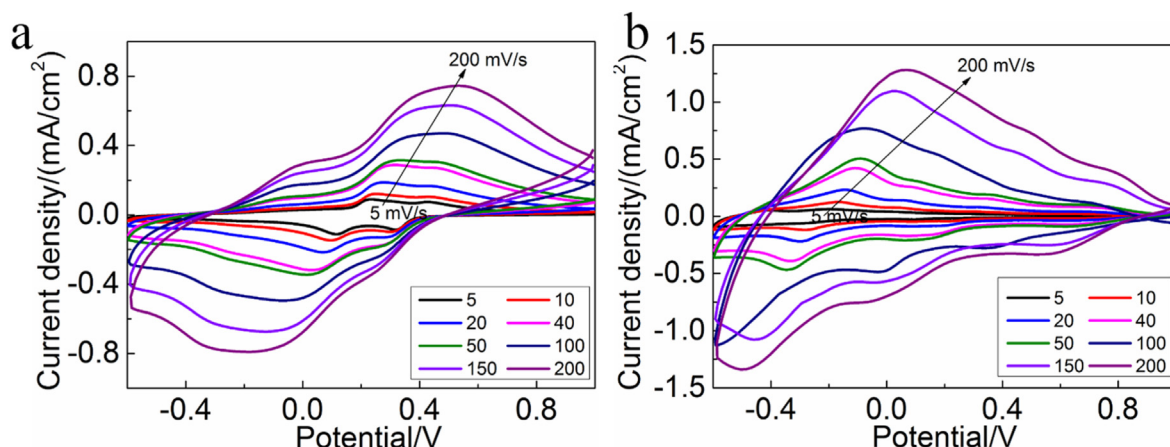


Fig. 5. CV curves of pristine V_2O_5 and V_2O_5 -nb film in 1.0 M $LiClO_4/PC$ solution under different scanning rates ranging from 5 to 200 mV/s.

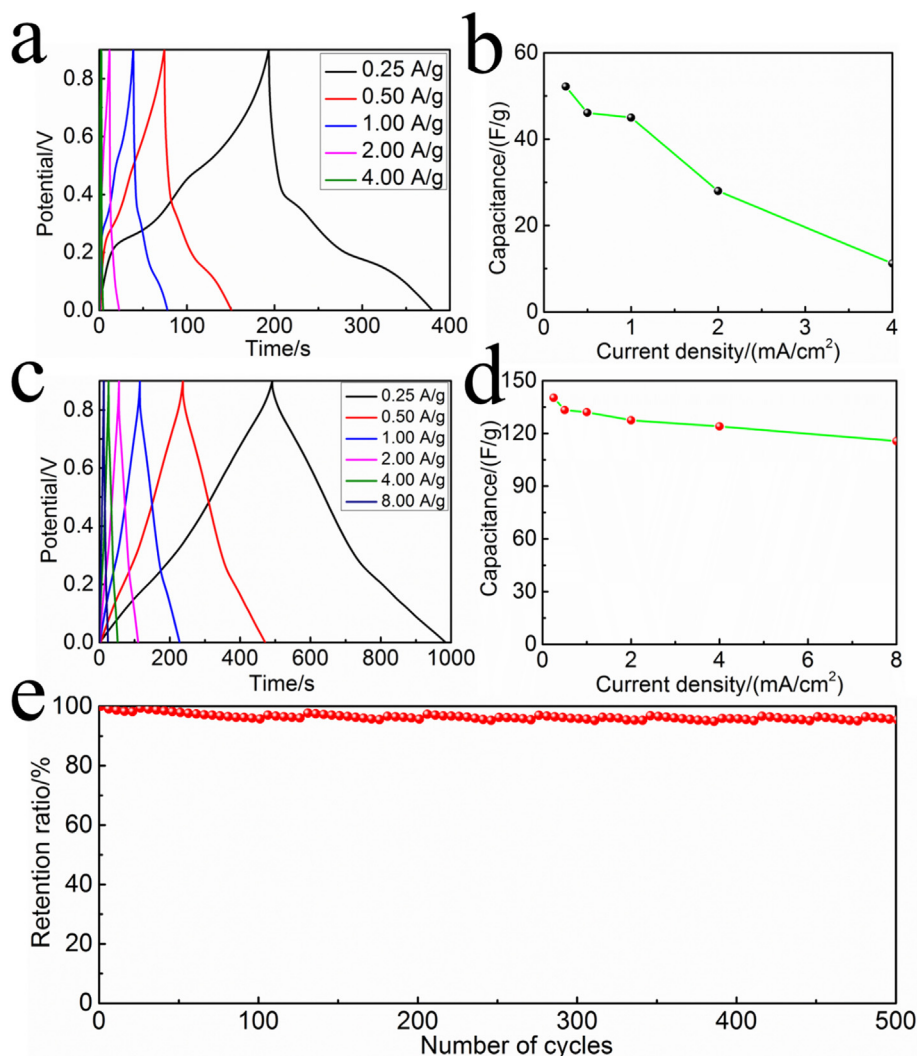


Fig. 6. Galvanostatic charge-discharge curves of commercial V_2O_5 (a) and V_2O_5 -nb (c) films at different current densities in 1 M $LiClO_4/PC$ solution. Effect of current density on capacitance for pristine V_2O_5 (b) and V_2O_5 -nb (d) films. (e) Galvanostatic charge-discharge cycling performance of V_2O_5 -nb film at a current density of 16 A/g in the potential range of 0–0.9 V.

shorten ion diffusion path and provide more active sites for charge-transfer reactions [50,51].

In order to demonstrate the level of stored energy can be simultaneously monitored by the visually detectable reversible color change of V_2O_5 -nb film, the galvanostatic charge-discharge curves corresponding in situ optical response curves under different current density at 490 nm for V_2O_5 -nb film was illustrated in Fig. 7 and Fig. S8. During the charging process, the color of the V_2O_5 -nb film changed gradually from yellow to brick-red. When the potential reached +0.9 V, the film got to fully colored state. During the discharging process, the color of the V_2O_5 -nb film changed gradually from brick-red to yellow. When the potential reached 0 V, the film got to fully bleached state. And even at a high current density of 16 A/g, the level of storage energy still can be monitored very well by the reversible and rapid color variation, as shown in Fig. 7b. It can be concluded that the V_2O_5 -nb film could be used as a promising energy storage material and simultaneously monitor the level of stored energy by visible color change.

In order to further demonstrate the advantages of solution-processable V_2O_5 nanobelts, the patterned electrochromic display with a large area of 36 cm^{-1} was successfully assembled. The solution-processable V_2O_5 nanobelts provide the possibility for

preparing large-scale and patterned electrochromic film by solution-processed techniques such as spray-coating and inkjet-printing. Here, the large-scale V_2O_5 -nb film ($6.0\text{ cm} \times 8.0\text{ cm}$) with a “No Smoking” pattern was successfully fabricated by spray-coating method. The all-solid-state large-scale electrochromic displays ($6.0\text{ cm} \times 6.0\text{ cm}$) with a “No Smoking” pattern was fabricated by using spray-coated V_2O_5 nanobelt film, $LiClO_4$ -PMMA-PC gel electrolyte, spray-coated PEDOT:PSS film as electrochromic layer, ion conductive layer and ion storage layer. The schematic illustrations of the patterned V_2O_5 -nb film and all-solid-state electrochromic displays were displayed in Fig. 8 a,b. The photographic images of large-scale patterned V_2O_5 -nb film under different potentials were displayed in Fig. 8 c-e. As the applied potential increased, the patterned V_2O_5 -nb film ($6.0\text{ cm} \times 8.0\text{ cm}$) exhibits a noticeable electrochromism and reversible multiple colors change from grey, yellow to brick-red. The photographs of patterned electrochromic displays ($6.0\text{ cm} \times 6.0\text{ cm}$) under different applied voltages were presented in Fig. 8 f-h. As the driving voltage increased, the large-scale patterned display also exhibits visible multiple colors, ranging from light green, red to black. And the patterned display sustains its colored and bleached states even when disconnecting to the power source, indicating it

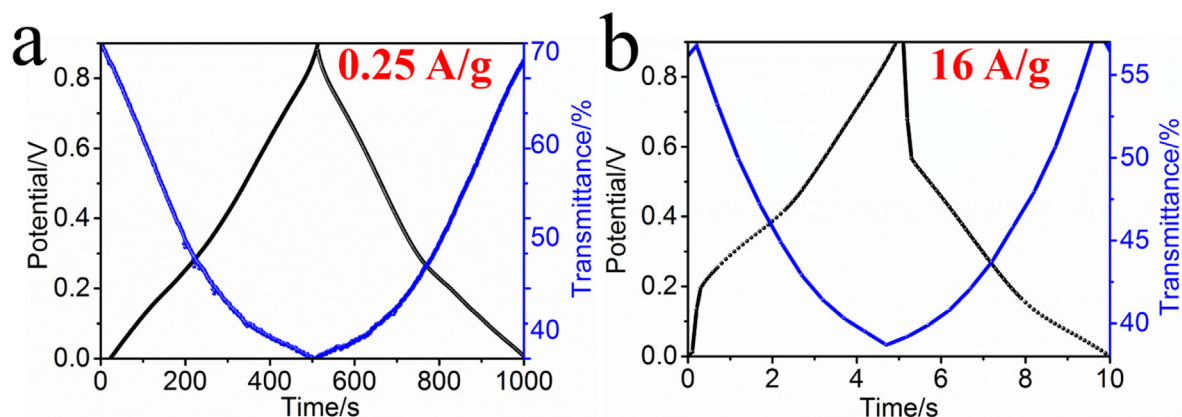


Fig. 7. Galvanostatic charge-discharge curves at 0.25 A/g (a) and 16 A/g (b) in the potential range of 0–0.9 V and corresponding in situ optical response at 490 nm for the V_2O_5 -nb films.

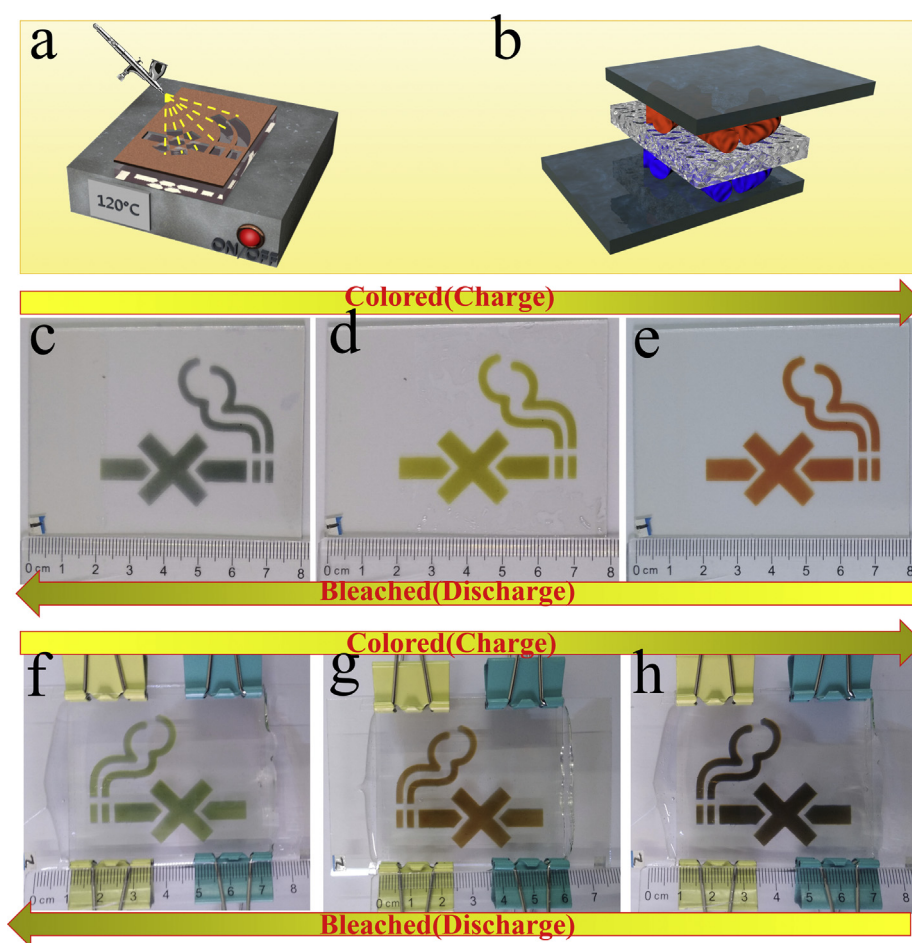


Fig. 8. Schematic illustration of the fabrication process of spray-processable patterned electrochromic film (a) and all-solid-state electrochromic displays (b). (c–e) Photographs of the patterned large-scale V_2O_5 -nb film under different potentials. (f–h) Photographic images of the patterned large-area electrochromic displays under different applied potentials.

as promising energy-saving device. Moreover, the patterned large-scale electrochromic display exhibits a large optical contrast of 61% at 530 nm, as illustrated in Fig. S9a. And the patterned display also exhibits fast response speed (below 2 s), as shown in Fig. S9b. The large-scale patterned display based on V_2O_5 -nb film exhibits excellent electrochromic performance and is a promising candidate for future energy-efficient displays.

4. Conclusions

The solution-processable V_2O_5 nanobelts with ultrahigh aspect ratio were successfully synthesized by a very simple and scalable method. The spray-coated V_2O_5 -nb film exhibits significantly improved electrochromic and electrochemical capacitance performance compared with commercial bulk V_2O_5 film. And the V_2O_5 -nb

film also shows long-term electrochromic cycling stability (sustaining 94% of its initial optical contrast after 1000 cycles) and electrochemical capacitance durability (capacitance decay of only 5% after 500 cycles). It is demonstrated that the level of stored energy for V_2O_5 -nb film could be simultaneously monitored by a reversible and rapid color change. Moreover, the large-scale patterned electrochromic display based on V_2O_5 -nb film exhibits multiple color changes, large optical modulation and fast switching speed. The solution-processable V_2O_5 nanobelts shows great promise as practical electrode materials for electrochromism and supercapacitor.

CRediT authorship contribution statement

Sihang Zhang: Conceptualization, Investigation, Writing - original draft, Writing - review & editing, Visualization. **Sheng Chen:** Resources, Supervision, Funding acquisition. **Yonghui Luo:** Visualization, Data curation, Formal analysis. **Bin Yan:** Formal analysis, Supervision. **Yingchun Gu:** Resources, Supervision. **Feng Yang:** Supervision, Project administration. **Ya Cao:** Resources, Supervision, Methodology.

Declaration of competing interest

The authors declare that they have no known competing financial interests or personal relationships that could have appeared to influence the work reported in this paper.

Acknowledgements

The authors gratefully acknowledge National Natural Science Foundation of China (contract no. 21876119 and 51721091) and Sichuan Province Science and Technology Foundation (2020YFG0094). We thank the Analytical and Testing Center of Sichuan University for material characterizations, and we also thank Prof. Hui Wang for her help of SEM tests, Prof. Yong Luo for his help of TEM tests and Prof. Yunfei Tian for his help of XPS tests.

Appendix A. Supplementary data

Supplementary data to this article can be found online at <https://doi.org/10.1016/j.jallcom.2020.155882>.

References

- [1] W. Wu, M. Wang, J. Ma, Y. Cao, Y. Deng, Electrochromic metal oxides: recent progress and prospect, *Adv. Electron. Mater.* 4 (2018) 1800185.
- [2] J. Li, Z. Liu, Q. Zhang, Y. Cheng, B. Zhao, S. Dai, H.H. Wu, K. Zhang, D. Ding, Y. Wu, Anion and cation substitution in transition-metal oxides nanosheets for high-performance hybrid supercapacitors, *Nanomater. Energy* 57 (2019) 22–33.
- [3] D. Majumdar, M. Mandal, S.K. Bhattacharya, V_2O_5 and its carbon-based nanocomposites for supercapacitor applications, *ChemElectroChem* 6 (2019) 1623–1648.
- [4] T.K. Le, M. Kang, S.W. Kim, A review on the optical characterization of V_2O_5 micro-nanostructures, *Ceram. Int.* 45 (2019) 15781–15798.
- [5] Y. Yue, H. Liang, Micro- and nano- structured vanadium pentoxide (V_2O_5) for electrodes of lithium-ion batteries, *Adv. Energy Mater.* 7 (2017) 1602545.
- [6] Y. Wei, Y. Ma, M. Chen, W. Liu, L. Li, Y. Yan, Electrochemical investigation of electrochromic device based on WO_3 and Ti doped V_2O_5 films by using electrolyte containing ferrocene, *J. Electroanal. Chem.* 807 (2017) 45–51.
- [7] I. Mjejri, M. Gaudon, A. Rougier, Mo addition for improved electrochromic properties of V_2O_5 thick films, *Sol. Energy Mater. Sol. Cells* 198 (2019) 19–25.
- [8] I. Mjejri, L.M. Mancieri, M. Gaudon, A. Rougier, F. Sediri, Nano-vanadium pentoxide films for electrochromic displays, *Solid State Ionics* 292 (2016) 8–14.
- [9] Y. Liu, C. Jia, Z. Wan, X. Weng, J. Xie, L. Deng, Electrochemical and electrochromic properties of novel nanoporous NiO/V_2O_5 hybrid film, *Sol. Energy Mater. Sol. Cells* 132 (2015) 467–475.
- [10] L. Deng, Y. Gao, Z. Ma, G. Fan, Free-standing graphene/vanadium oxide composite as binder-free electrode for asymmetrical supercapacitor, *J. Colloid Interface Sci.* 505 (2017) 556–565.
- [11] T. Kim, H. Kim, T.S. You, J. Kim, Carbon-coated V_2O_5 nanoparticles derived from metal-organic frameworks as a cathode material for rechargeable lithium-ion batteries, *J. Alloys Compd.* 727 (2017) 522–530.
- [12] M. Yan, L. Zhao, K. Zhao, Q. Wei, Q. An, G. Zhang, X. Wei, W. Ren, L. Mai, The capturing of ionized oxygen in sodium vanadium oxide nanorods cathodes under operando conditions, *Adv. Funct. Mater.* 26 (2016) 6555–6562.
- [13] D. Huo, B. Laik, P. Bonnet, K. Guérin, C. Cenac-Morthe, R. Baddour-Hadjean, J. Pereira-Ramos, Understanding of the nanosize effect on the structure and electrochemistry of V_2O_5 obtained via fluorine chemistry, *Mater. Today Proceedings* 5 (2018) 22850–22858.
- [14] F.A. Tabar, F. Sharif, S. Mazinani, Preparation and electrochemical performance of a novel three dimensional structure of polyaniline hollow fibers decorated by graphene, *Polymer* 154 (2018) 80–89.
- [15] X. Wang, Z. Li, J. Shi, Y. Yu, One-dimensional titanium dioxide nanomaterials: nanowires, nanorods, and nanobelts, *Chem. Rev.* 114 (2014) 9346–9384.
- [16] S. Hussain, X. Yang, M.K. Aslam, A. Shaheen, M.S. Javed, N. Aslam, B. Aslam, G. Liu, G. Qiao, Robust TiN nanoparticles polysulfide anchor for Li–S storage and diffusion pathways using first principle calculations, *Chem. Eng. J.* (2019) 123595.
- [17] X. Zhang, S. Dou, W. Li, L. Wang, H. Qu, X. Chen, L.X. Zhang, Y. Zhao, J. Zhao, Y. Li, Preparation of monolayer hollow spherical tungsten oxide films with enhanced near infrared electrochromic performances, *Electrochim. Acta* 297 (2019) 223–229.
- [18] R. André, F. Natálio, M. Humanes, J. Leppin, K. Heinze, R. Wever, H.C. Schröder, W.E. Müller, W. Tremel, V_2O_5 nanowires with an intrinsic peroxidase-like activity, *Adv. Funct. Mater.* 21 (2011) 501–509.
- [19] Z. Tong, N. Li, H. Lv, Y. Tian, H. Qu, X. Zhang, J. Zhao, Y. Li, Annealing synthesis of coralline V_2O_5 nanorod architecture for multicolor energy-efficient electrochromic device, *Sol. Energy Mater. Sol. Cells* 146 (2016) 135–143.
- [20] J.S. Bonso, A. Rahy, S.D. Perera, N. Nour, O. Seitz, Y.J. Chabal, K.J. Balkus Jr., J.P. Ferraris, D.J. Yang, Exfoliated graphite nanoplatelets– V_2O_5 nanotube composite electrodes for supercapacitors, *J. Power Sources* 203 (2012) 227–232.
- [21] N. Wang, Y. Zhang, T. Hu, Y. Zhao, C. Meng, Facile hydrothermal synthesis of ultrahigh-aspect-ratio V_2O_5 nanowires for high-performance supercapacitors, *Curr. Appl. Phys.* 15 (2015) 493–498.
- [22] D. Yu, C. Chen, S. Xie, Y. Liu, K. Park, X. Zhou, Q. Zhang, J. Li, G. Cao, Mesoporous vanadium pentoxide nanofibers with significantly enhanced Li-ion storage properties by electrospinning, *Energy Environ. Sci.* 4 (2011) 858–861.
- [23] X. Li, K. Perera, J. He, A. Gumyusenge, J. Mei, Solution-processable electrochromic materials and devices: roadblocks and strategies towards large-scale applications, *J. Mater. Chem. C* 7 (2019) 12761–12789.
- [24] S. Zhang, Y. Zhao, Z. Du, Y. Luo, S. Chen, Y. Gu, B. Yan, F. Yang, Y. Cao, Solution-processable three-dimensional honeycomb-like poly (3, 4-ethylenedioxythiophene) nanostructure networks with very fast response speed for patterned electrochromic devices, *Sol. Energy Mater. Sol. Cells* 207 (2020) 110354.
- [25] K. Karthik, M.P. Nikolova, A. Phuruangrat, S. Pushpa, V. Revathi, M. Subbulakshmi, Ultrasound-assisted synthesis of V_2O_5 nanoparticles for photocatalytic and antibacterial studies, *Mater. Res. Innovat.* (2019) 1–6.
- [26] K. Zhang, N. Li, X. Ma, Y. Wang, J. Zhao, L. Qiang, X. Li, Y. Li, Building ultrathin polyaniline encapsulated V_2O_5 heterogeneous nanowires and its electrochromic performance, *J. Electroanal. Chem.* 825 (2018) 16–21.
- [27] X. Rui, Y. Tang, O.I. Malyi, A. Gusak, Y. Zhang, Z. Niu, H.T. Tan, C. Persson, X. Chen, Z. Chen, Ambient dissolution–recrystallization towards large-scale preparation of V_2O_5 nanobelts for high-energy battery applications, *Nanomater. Energy* 22 (2016) 583–593.
- [28] D. Kong, X. Li, Y. Zhang, X. Hai, B. Wang, X. Qiu, Q. Song, Q.H. Yang, L. Zhi, Encapsulating V_2O_5 into carbon nanotubes enables the synthesis of flexible high-performance lithium ion batteries, *Energy Environ. Sci.* 9 (2016) 906–911.
- [29] G. Silversmit, D. Depla, H. Poelman, G.B. Marin, R. De Gryse, Determination of the V_{2p} XPS binding energies for different vanadium oxidation states (V^{5+} to V^{0+}), *J. Electron. Spectrosc. Relat. Phenom.* 135 (2004) 167–175.
- [30] J. Mendialdua, R. Casanova, Y. Barbaux, XPS studies of V_2O_5 , V_6O_{13} , VO_2 and V_2O_3 , *J. Electron. Spectrosc. Relat. Phenom.* 71 (1995) 249–261.
- [31] S. Sajitha, U. Aparna, B. Deb, Ultra-thin manganese dioxide-encrusted vanadium pentoxide nanowire mats for electrochromic energy storage applications, *Adv. Mater. Interfaces* 6 (2019) 1901038.
- [32] M. Benmoussa, A. Outzourhit, A. Bennouna, E. Ameziene, Electrochromism in sputtered V_2O_5 thin films: structural and optical studies, *Thin Solid Films* 405 (2002) 11–16.
- [33] S. Liu, X. Zhang, P. Sun, C. Wang, Y. Wei, Y. Liu, Enhanced electrochromic properties of a TiO_2 nanowire array via decoration with anatase nanoparticles, *J. Mater. Chem. C* 2 (2014) 7891–7896.
- [34] Y. Chen, Z. Bi, X. Li, X. Xu, S. Zhang, X. Hu, High-coloration efficiency electrochromic device based on novel porous $TiO_2@$ prussian blue core-shell nanostructures, *Electrochim. Acta* 224 (2017) 534–540.
- [35] G. Cai, J. Tu, D. Zhou, J. Zhang, X. Wang, C. Gu, Dual electrochromic film based on WO_3 /polyaniline core/shell nanowire array, *Sol. Energy Mater. Sol. Cells* 122 (2014) 51–58.
- [36] G. Cai, P. Darmawan, X. Cheng, P.S. Lee, Inkjet printed large area multifunctional smart windows, *Adv. Energy Mater.* 7 (2017) 1602598.
- [37] J. Zhang, J.P. Tu, D. Zhang, Y.Q. Qiao, X.H. Xia, X.L. Wang, C.D. Gu, Multicolor

- electrochromic polyaniline–WO₃ hybrid thin films: one-pot molecular assembling synthesis, *J. Mater. Chem.* 21 (2011) 17316–17324.
- [38] A. Chaudhary, D.K. Pathak, M. Tanwar, P. Yogi, P.R. Sagdeo, R. Kumar, Polythiophene–PCBM-based all-organic electrochromic device: fast and flexible, *ACS Appl. Electron. Mater.* 1 (2019) 58–63.
- [39] S. Hussain, N. Ullah, Y. Zhang, A. Shaheen, M.S. Javed, L. Lin, Zulfiqar, S.B. Shah, G. Liu, G. Qiao, One-step synthesis of unique catalyst Ni₉S₈@C for excellent MOR performances, *Int. J. Hydrogen Energy* 44 (2019) 24525–24533.
- [40] B.G. Choi, M. Yang, W.H. Hong, J.W. Choi, Y.S. Huh, 3D macroporous graphene frameworks for supercapacitors with high energy and power densities, *ACS Nano* 6 (2012) 4020–4028.
- [41] G. Cai, X. Wang, M. Cui, P. Darmawan, J. Wang, A.L.-S. Eh, P.S. Lee, Electrochromo-supercapacitor based on direct growth of NiO nanoparticles, *Nanomater. Energy* 12 (2015) 258–267.
- [42] S.C. Dhanabalan, J.S. Ponraj, H. Zhang, Q. Bao, Present perspectives of broadband photodetectors based on nanobelts, nanoribbons, nanosheets and the emerging 2D materials, *Nanoscale* 8 (2016) 6410–6434.
- [43] B. Wang, J.S. Chen, Z. Wang, S. Madhavi, X.W. Lou, Green synthesis of NiO nanobelts with exceptional pseudo-capacitive properties, *Adv. Energy Mater.* 2 (2012) 1188–1192.
- [44] G. Cai, P. Darmawan, M. Cui, J. Wang, J. Chen, S. Magdassi, P.S. Lee, Highly stable transparent conductive silver grid/PEDOT: PSS electrodes for integrated bifunctional flexible electrochromic supercapacitors, *Adv. Energy Mater.* 6 (2016) 1501882.
- [45] G. Cai, J. Tu, D. Zhou, J. Zhang, Q. Xiong, X. Zhao, X. Wang, C. Gu, Multicolor electrochromic film based on TiO₂@polyaniline core/shell nanorod array, *J. Phys. Chem. C* 117 (2013) 15967–15975.
- [46] G. Cai, J. Tu, J. Zhang, Y.J. Mai, Y. Lu, C.D. Gu, X. Wang, An efficient route to a porous NiO/reduced graphene oxide hybrid film with highly improved electrochromic properties, *Nanoscale* 4 (2012) 5724–5730.
- [47] R. Yuksel, S. Coskun, G. Gunbas, A. Cirpan, L. Toppare, H.E. Unalan, Silver nanowire/conducting polymer nanocomposite electrochromic supercapacitor electrodes, *J. Electrochem. Soc.* 164 (2017) A721–A727.
- [48] H. Wei, J. Zhu, S. Wu, S. Wei, Z. Guo, Electrochromic polyaniline/graphite oxide nanocomposites with endured electrochemical energy storage, *Polymer* 54 (2013) 1820–1831.
- [49] G. Cai, X. Cheng, M. Layani, A.W.M. Tan, S. Li, A.L. Eh, D. Gao, S. Magdassi, P.S. Lee, Direct inkjet-patterning of energy efficient flexible electrochromics, *Nanomater. Energy* 49 (2018) 147–154.
- [50] S. Hussain, M.S. Javed, S. Asim, A. Shaheen, A.J. Khan, Y. Abbas, N. Ullah, A. Iqbal, M. Wang, G. Qiao, Novel gravel-like NiMoO₄ nanoparticles on carbon cloth for outstanding supercapacitor applications, *Ceram. Int.* 46 (2020) 6406–6412.
- [51] Z. Wang, H. Qiang, C. Zhang, Z. Zhu, M. Chen, C. Chen, D. Zhang, Facile fabrication of hollow polyaniline spheres and its application in supercapacitor, *J. Polym. Res.* 25 (2018) 129.